AIMS Energy, 12(6): 1334–1365.
DOI: 10.3934/energy.2024060
Received: 04 September 2024
Revised: 25 November 2024
Accepted: 09 December 2024
Published: 23 December 2024

http://www.aimspress.com/journal/energy

Research article

Piezoelectric energy harvesting under free and forced vibrations for different operating conditions

Amine Ben Alaya[1,*] Charfeddine Mrad[2], and Férid Kourda[1]

[1] Laboratory of Electrical Systems (LR-11-ES15), National Engineering School of Tunis, University of Tunis El Manar, Tunis, 1068, Tunisia
[2] Laboratory of Applied Mechanics and Engineering, National Engineering School of Tunis, University of Tunis El Manar, Tunis, 1068, Tunisia

* **Correspondence:** Email: amine.ben.alaya.LSE@gmail.com; Tel: +0021653114713.

Abstract: The field of energy harvesting has grown rapidly, with the huge development in low-power devices and the Internet of Things (IoT). With the intent of harvesting electrical energy for self-powered devices, piezoelectric technology is considered. In this study, we proposed several electrical and mechanical improvements to enhance the electrical energy produced through piezoelectricity. To determine the best electrical configuration to harvest piezoelectric energy, three harvesting electric circuits were proposed and tested using a piezoelectric material (PZT-5H) mounted directly on a vibration exciter. The harvested electrical energy by each circuit was determined at different excitation frequencies, from 20 to 50 Hz, with an excitation amplitude of 2 mm. The favorable electric circuit produced approximately 35 µJ of electrical energy at an excitation frequency of 50 Hz. This circuit was subsequently used for the remaining aspects of this work. To enhance the obtained electrical energy, a fixed-free metallic plate was used. First, free vibration was tried, imposing an excitation displacement of different values to the free end of the plate. The plate consisted of different materials: copper, aluminum, and steel. The PZT-5H was mounted at different positions on the plate. The harvested electrical energy was determined for each plate material, each piezoelectric material position, and each excitation displacement. The highest harvested energy was around 6 µJ. Second, forced vibration was tried, imposing an excitation amplitude of 0.5 mm at different excitation frequencies, from 10 to 50 Hz, to the fixed end of the plate. The plate was of different lengths. The highest harvested energy was around 540 µJ. Third, we showed that it is possible to further increase the harvested electrical energy by tuning the plate resonance to 50 Hz. The harvested

energy was then around 1010 μJ. The obtained results allowed optimizing piezoelectric energy harvesting toward supplying low-power devices for different applications.

Keywords: energy harvesting; piezoelectricity; free vibration; forced vibration; operating parameters

1. Introduction

With the expeditious development of the Internet of Things (IoT) [1,2] and wireless technology [3,4], the field of renewable energy [5–8] has recently become one of the most significant areas of research. Toka et al. [9] improved the electrical and thermal performance of photovoltaic-thermal (PVT) systems integrated into buildings. Implementing this solution represents one of the methods that involves the upcoming studies on renewable energy and eco-friendly products [10,11], aiming to assess their environmental impact [12,13]. Energy harvesting [14–16] is a way to generate electricity from ambient energy sources, such as sunlight, wind, and vibration. This electricity can be used to power small electronic devices, such as sensors, wearables, and remote monitoring systems. Dai et al. [17] explored the effect of electric fields produced by energy-harvesting phenomena on the performance of photocatalytic technologies. Energy-harvesting technologies have been developed based on a variety of energy conversion phenomena, including piezoelectricity [18,19], electrostatics [20,21], electromagnetism [22,23], triboelectricity [24,25], and pyroelectricity which can be exploited to enhance photocatalytic performance [26]. Piezoelectric materials are a promising source of energy harvesting, as they can produce power ranging from nanowatts to microwatts. The word "piezoelectricity" emanated from two words, "piezo", meaning the principle of stress, and "electricity", meaning dependable on electron movement [27]. Piezoelectricity is the capability of particular materials to produce an electric field when squeezed or pressed, and vice versa. Nowadays piezoelectric materials are used in a variety of practical applications. Zou et al. [28] employed piezoelectricity to design sensors for monitoring physiological parameters. This technology can be used to fabricate COVID-19 detectors, air pollutant detectors, and solution measurement devices [29]. Based on the literature, piezoelectric energy harvesting was created with the main purpose of conversion efficiency [30,31], output power [32,33], and bandwidth [34,35]. Li et al. [36] classified piezoelectric materials into four categories: composites, polymers, single crystals, and ceramics, and compared their piezoelectric properties, including piezoelectric strain constant (S), electromechanical coupling factor (k), piezoelectric voltage constant (g), mechanical quality factor (Q), and the dielectric constant, to those of other key candidate materials. Han et al. [37] presented piezoelectric paint sensors, defined their concept, potential applications, and methods of preparation. They also highlighted the historical development of these sensors, emphasizing their advantages, such as flexibility and ease of installation, and exploring their growing relevance in different fields. Maurya et al. [38] developed a high energy density harvester based upon an organic piezoelectric material to power wireless data transfer, which was able to power 78 LEDs. Rupp et al. [39] opened the way for the use of topology optimization to design piezoelectric energy harvesting systems (PEHs) with improved output power under harmonic excitation. They demonstrated that the piezoelectric patch must be topologically optimized to alter the structural modes and tune the structure to the driving frequency while preventing charge cancellation. Lefeuvre et al. [40] provided a comparison between several vibration-powered piezoelectric generators for stand-alone

systems and they detailed the principle of each processing circuit. Song et al. [41] proposed a PEH with a double-cantilever beam (DCB) undergoing coupled bending-torsion vibrations, by combining the width-splitting method and asymmetric mass, for more ambient energy harvesting from environmental vibration with multiple frequency excitation. Baek et al. [42] employed a facile form of the hydrothermal synthesis method to obtain BaZrxTi1xO3 (BZT) nanoparticles (NPs) with a wide range of Zr concentrations. The BZT NP-embedded piezoelectric energy harvester (PEH) with a Pb concentration of 32 mol% consistently harvested a stable recovered voltage of 20 V and a current of 400 nA. Han et al. [43] proposed a bimorph structure to effectively integrate and improve the performance of a flexible PZT thin-film energy harvester as a single device configuration. The electrical outputs reached in this study demonstrate improved performance, with a voltage achieving close to 280 V and a maximum current up to 2.2 μA. Lee et al. [44] presented a piezoelectric composite energy harvester attached inside a tire to convert longitudinal tire strain into electrical power. The harvester, with dimensions 60 × 100 × 3 mm, can generate a power density of 1.37 $\mu W/mm^3$, enough to power a wireless sensor. Baker et al. [45] proved that, for three different types of piezoelectric materials, the 33 mode has a higher coupling coefficient k, than the 31 mode. An additional study comparing the performance of piezoelectric, electromagnetic, and electrostatic energy generation methods was realized by Sterken et al. [46]. Each power generation technique was modeled mathematically and compared. In this study, we propose several electrical and mechanical improvements to enhance the electrical energy harvested through piezoelectricity. To determine the best electrical configuration to harvest piezoelectric energy, three harvesting circuits are proposed and tested using a piezoelectric material (PZT-5H) mounted directly on a vibration exciter. The harvested electrical energy by each circuit is determined at different excitation frequencies (20 to 50 Hz). The best circuit is then used to characterize the piezoelectric material. To improve the obtained electrical energy, a fixed-free metallic plate is used. First, free vibration is tried, imposing an excitation displacement of different values to the free end of the plate for different materials: copper, aluminum, and steel. The piezoelectric material is mounted at different positions on the plate. The harvested electrical energy is determined for each plate material, each piezoelectric material position, and each excitation displacement. Second, forced vibration is tried at different excitation frequencies (20 to 50 Hz) at the fixed end of the plate, which is of different lengths. Third, we show that it is possible to further improve the harvested electrical energy by tuning the plate resonance to 50 Hz. The obtained results allow optimizing piezoelectric energy harvesting toward supplying low-power devices.

2. Materials and methods

2.1. Piezoelectric material

2.1.1. Description

To generate electricity from mechanical vibration, we used a piezoelectric ceramic component made of lead zirconate titanate (PZT-5H). PZT-5H is a soft piezoelectric ceramic with high sensitivity. It is chemically defined as: (Pb1.0[Zr0.49Ti0.46(Li0.25Sb0.75)0.05]O3) [47]. Figure 1a shows the PZT-5H component, Figure 1b presents the front view, Figure 1c depicts the right-side

view within a cross-section, and Figure 1d illustrates the bottom view within a cross-section. Table 1 highlights the key properties of PZT-5H.

Table 1. Properties of the piezoelectric material (PZT 5-H) [48,49].

Capacity (pF)	Resonance frequency (Hz)	Resonance impedance (Ω)	d_{33} (pC/N)	g_{33} (m^2/C)	d_{31} (pC/N)
30,000 ± 30%	3000 ± 400	≥ 600	593	20×10^{-3}	−274

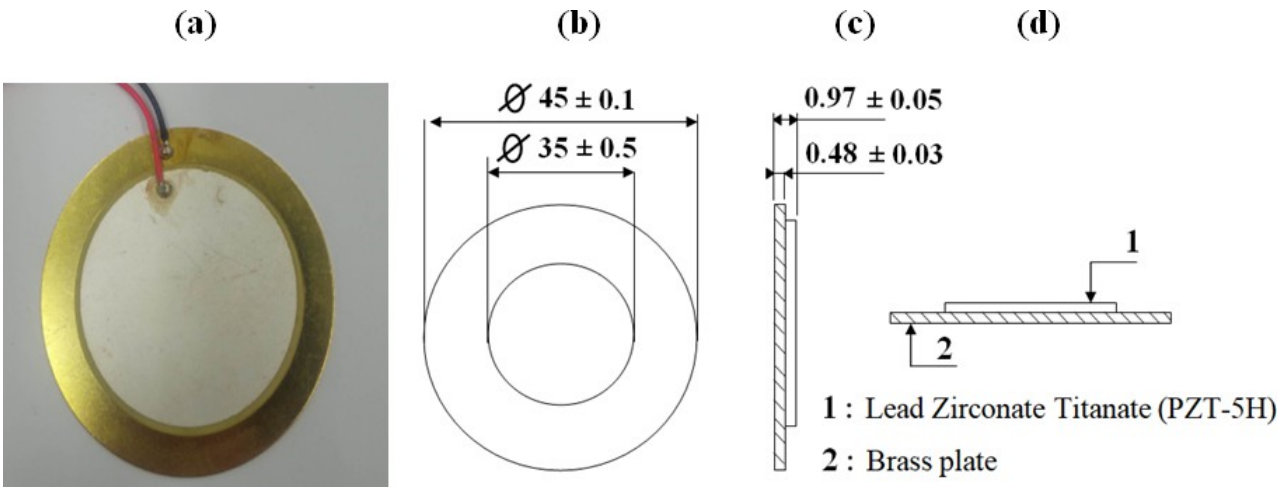

Figure 1. Piezoelectric material used: (a) PZT-5H component, (b) front view, (c) right-side view within a cross-section, (d) bottom view within a cross-section.

2.1.2. Theory

In this work, the piezoelectric material is subjected to vibrational energy in the direction 3, leading to an investigation of the d_{33} coefficient to analyze its response. The different parameters of PZT-5H are shown in Figure 2.

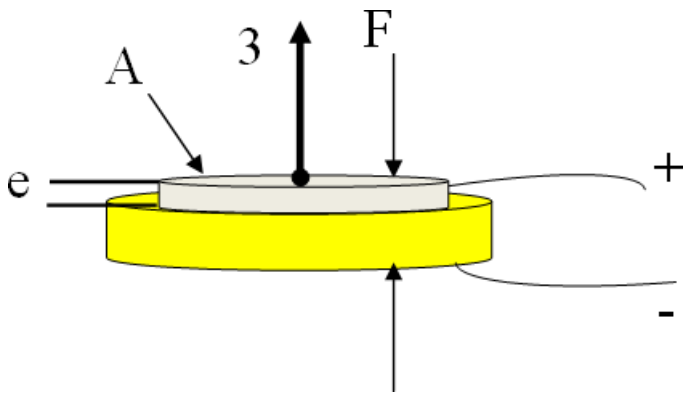

Figure 2. PZT-5H subjected to mechanical force in direction 3.

The main equation that defines the electrical polarization as a function of the vibration applied force on the piezoelectric material is expressed by the following equation [50]:

$$P_3 = d_{33}T_3 \tag{1}$$

where P_3 ($C/m2$) is the electrical polarization, d_{33} (C/N) is the piezoelectric coefficient, and T_3 (MPa) is the mechanical stress.

The capacitance of the piezoelectric material is defined by the following equation:

$$C = \varepsilon_0\varepsilon_r \frac{A}{e} \tag{2}$$

where C (F) is the capacitance of the piezoelectric material, ε_0 (F/m) is the vacuum permittivity, ε_r is the relative permittivity, A (m^2) is the piezoelectric material area, and e (m) is the material thickness.

The produced voltage via piezoelectric material is given by the following equation:

$$U_p = Q/C \tag{3}$$

where U_p (V) is the produced voltage and Q (C) is the electric charge.

The relation between electric charge and applied force is given by the following equation:

$$Q_3 = d_{33}F_3 \tag{4}$$

where F_3 (N) is the vibration applied force in the direction 3.

The vibration force applied to the piezoelectric material is calculated as follows:

$$F_3 = ma = mX \times (2\pi f)^2 \tag{5}$$

where m (Kg) is the mass of the vibratory component, a (m/s^2) is the vibration acceleration, X (m) is the excitation amplitude, and f (Hz) is the vibration frequency.

The recovered voltage is therefore expressed as follows:

$$U_p = \frac{d_{33} \cdot m \cdot X \cdot e \cdot (2\pi f)^2}{\varepsilon_0 \,.\, \varepsilon_r \,.\, A} \tag{6}$$

Hence, we can confirm that the voltage generated by a piezoelectric material is directly dependent on the applied force, and consequently on the vibration frequency and the vibration amplitude. When the applied force, the vibration amplitude, or the vibration frequency increase, the produced voltage via piezoelectricity increase consequently.

2.2. Plates used

To study the electrical energy harvested at free excitation, we used three vibrating plates. The plates are shown in Figure 3. They are of ordinary steel, copper, and aluminum. The plates functional dimensions are: length = 150 mm, width = 65 mm, and thickness = 0.5 mm. To study the electrical energy harvested at forced excitation, we used five vibrating plates. The plates are presented in Figure 4, and are made of ordinary steel. The functional plate lengths are: 315, 255, 225, 170, and 145 mm. The width and the thickness are, respectively, 65 and 1.25 mm.

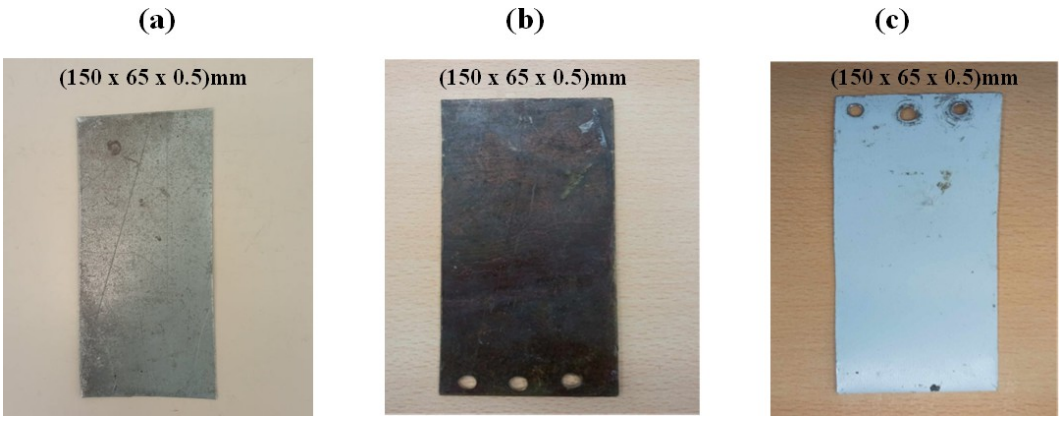

Figure 3. Plate materials: (a) steel, (b) copper, (c) aluminum.

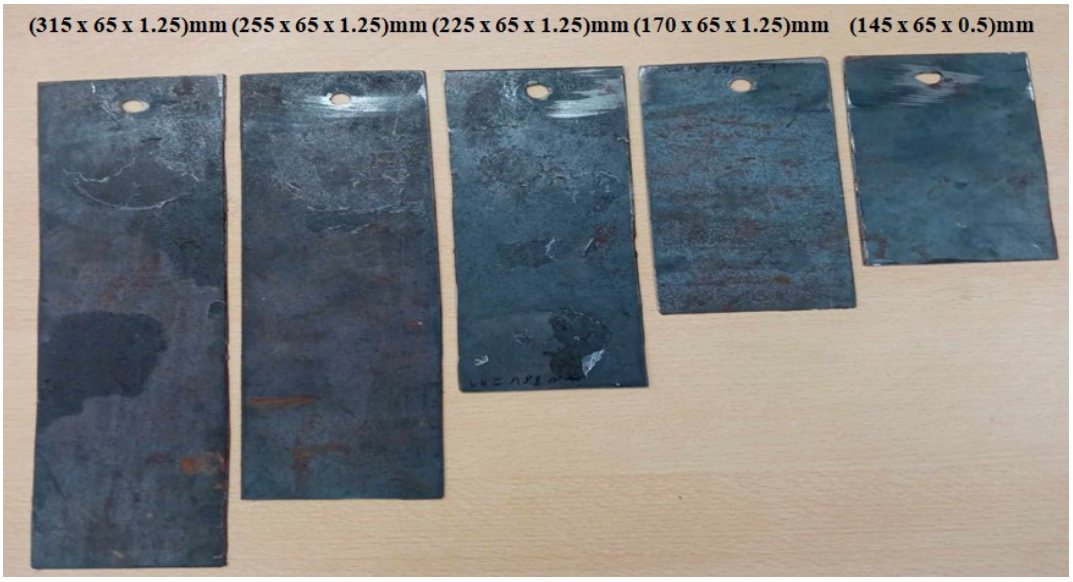

Figure 4. Steel plate lengths : 315, 255, 225, 170, 145 mm.

2.3. Experimental setup

To quantify the electrical energy harvested by the piezoelectric effect for all configurations, we employed an experimental setup that converts mechanical energy into electrical energy via vibrational frequency. The components of the experimental setup are as follows:

-Figure 5a: The amplitude amplifier, which serves to adjust the vibration magnitude.

-Figure 5b: The vibration exciter, which is utilized to generate mechanical vibrations.

-Figure 5c: The numerical oscilloscope, which is employed to visualize the electrical voltage.

-Figure 5d: The frequency regulator, which is adopted to set the vibration frequency.

-Figure 5e: The Schottky diodes (1N5817), which are exploited to rectify the produced voltage.

-Figure 5f: The electric test plate, which contains the different electric components.

-Figure 5g: The experimental setup, which presents the experimental layout.

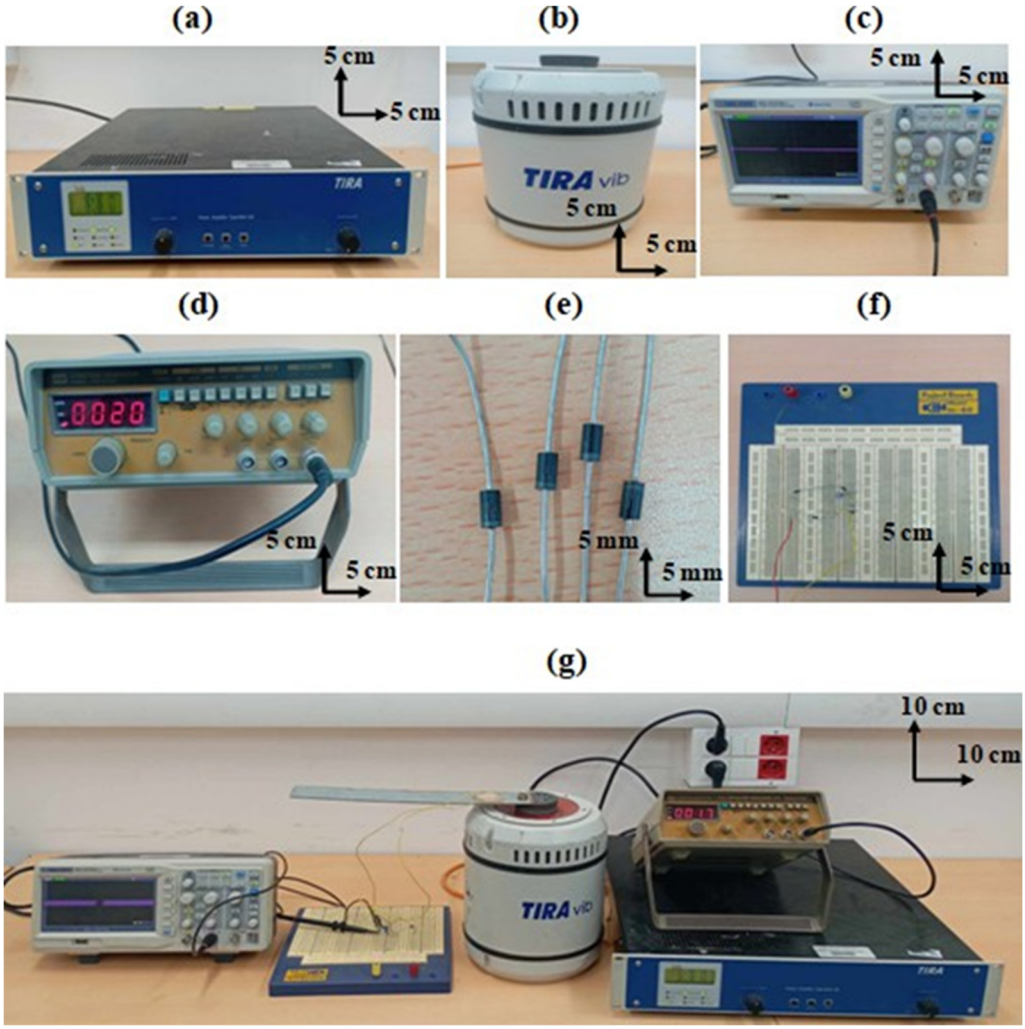

Figure 5. Experimental components: (a) amplitude amplifier, (b) vibration exciter, (c) oscilloscope, (d) frequency regulator, (e) Schottky diodes, (f) electric test plate, (g) experimental setup.

2.4. Reference parameters

- Produced voltage (U)

  It is the voltage produced by the piezoelectric disk, displayed on the oscilloscope.

- Stored energy (W)

  It is the energy stored in the capacitor (C = 1 μF), defined as:

$$W_p = 1/2\ CU_p^2 \tag{7}$$

where W_p (μJ) is the generated energy, U_p (V) is the generated voltage, and C (F) is the capacitance of the electric circuit.

- Excitation amplitude X (mm)

It is the amplitude at forced vibration, imposed by the exciter at the fixed end of the plate. It is shown on the amplitude amplifier X.

- Excitation frequency f (Hz)

It is the vibration frequency, noted on the frequency regulator. The frequency is between 20 and 50 Hz for evaluating the electrical circuits and the piezoelectric disk, and is between 10 and 50 Hz elsewhere.

- Natural frequency f_n (Hz)

It is the frequency at which the plates oscillate with large amplitude. The natural frequency was determined experimentally using the experimental setup, numerically using Abacus software, and analytically using the following formula:

$$f_n = \frac{\gamma_n}{2\pi L^2}\left(\frac{E I}{\rho h b}\right)^{\frac{1}{2}} \quad (8)$$

where γ_n (no unit) is the coefficient of the vibration mode and boundary conditions, L (m) is the plate length, b (m) is the plate width, E (Pa) is the Young modulus, h (m) is the plate thickness, ρ (Kg/m^3) is the volumetric mass, and I (m^4) is the quadratic moment.

- Charging time T (s)

It is the time required by the capacitor to reach full charge, and is displayed on the oscilloscope.

- Excitation displacement d (mm)

It is the excitation amplitude at free vibration, obtained by pushing the free end of the plate.

- Disk position P (mm)

It is the position of the piezoelectric material on the vibrating plates relative to the embedded end.

2.5. Harvesting circuit

The piezoelectric material generates both positive and negative voltages, which vary with the vibration amplitude. These voltages are rectified by Schottky diodes. However, this process introduces a voltage drop equal to $2V_{Dsat}$, where V_{Dsat} is the saturation voltage of the diode. In this study, we used Schottky diodes (1N5817) to minimize the voltage drop, as its drop is typically around 0.6 to 0.8 V, compared to 1 to 1.5 V for fast PN junction diodes. The Schottky diodes employed are capable of withstanding up to 20 V in reverse bias and 1 A in forward bias. For all electric configurations used in this work, the alternating voltage produced by the piezoelectric material is rectified by Schottky diodes, and then smoothed and stored. Therefore, there is no need for a resistance to determine the

produced energy, as in references [51] and [52], where the produced power and current are not studied. The different circuits proposed in this work are as follows:

- Circuit A

This electric circuit contains two Schottky diodes, a capacitor, and the PZT-5H. In this configuration, there is only one voltage drop, which improve the energy production. The diagram of this circuit is illustrated in Figure 6. The electrical energy recovered through this configuration is defined in Eq 7.

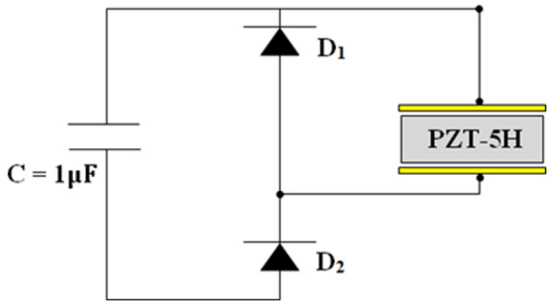

Figure 6. Circuit with two diodes and a capacitor.

- Circuit B

This circuit was employed in different studies on electrical energy harvested by the piezoelectric effect. It contains a Schottky diode bridge, the piezoelectric material, and a capacitor. The diagram of this circuit is presented in Figure 7. The electrical energy recovered through this configuration is defined in Eq 7.

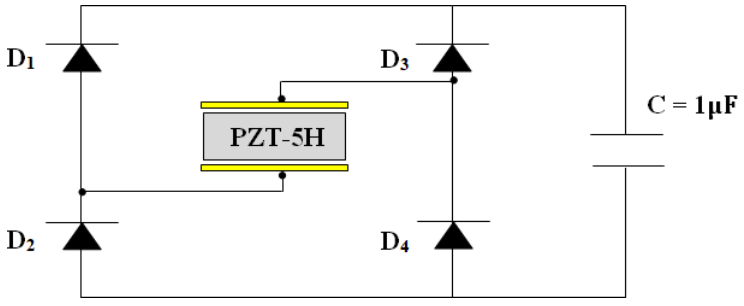

Figure 7. Basic circuit of the piezoelectric energy harvester system.

- Circuit C

In this configuration, we utilized a voltage doubling rectifier, where there is only one voltage drop for each positive or negative half-cycle. In traditional electronic circuits, the voltage is doubled relative to the input amplitude for a generator producing an alternating voltage. However, in this

configuration, each capacitor stores energy (W_1 and W_2) which is discharged into capacitor C_3. The electrical energy harvested through this configuration is defined as follows:

$$W_p = 1/2\ U_p\ C_T{}^2 \tag{9}$$

where C_T (μF) is the total circuit capacity of 1.11 μF. The diagram of this circuit is presented in Figure 8.

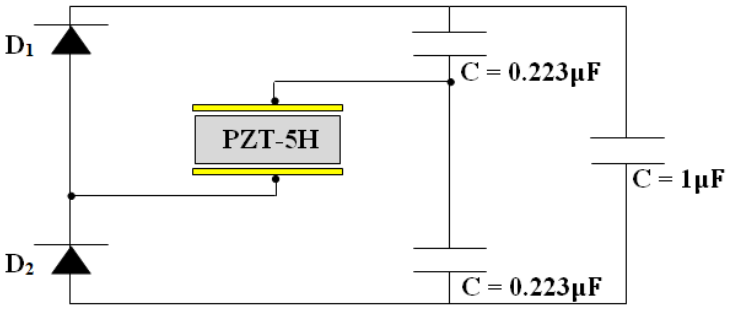

Figure 8. Circuit with two diodes and three capacitors.

2.6. Mechanical excitation

2.6.1. Setup without the vibrating plate

The conversion of mechanical energy into electrical energy is conducted by the direct application of vibrational energy to the piezoelectric material. The PZT-5H is securely bonded on the vibration exciter using an epoxy adhesive (EP-HP1500-FR). The principle of direct excitation is presented in Figure 9.

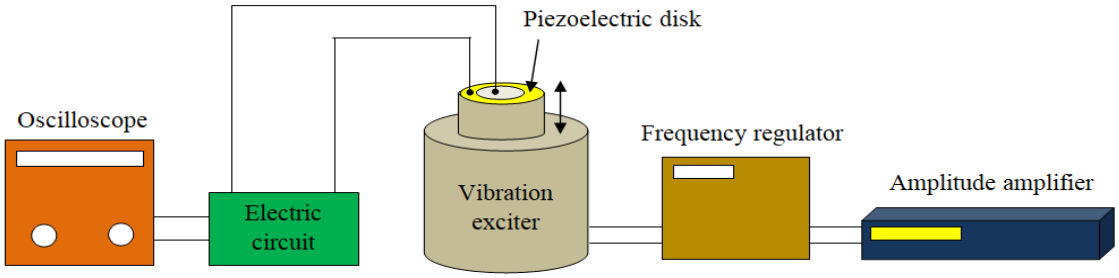

Figure 9. Direct excitation experimental setup.

2.6.2. Setup with a vibrating plate

The conversion of mechanical energy into electrical energy is conducted by the indirect application of vibrational energy to the piezoelectric material. The PZT-5H is securely bonded on the vibrating plate using an epoxy adhesive (EP-HP1500-FR). The principle of indirect excitation is presented in Figures 10 and 11.

- Free excitation

The vibrating plate is fixed-free. It is pushed on the free end in order to impose a displacement, and then released to initiate free vibration. The harvested electrical energy is subsequently determined as a function of the imposed displacement and as a function of the piezoelectric disk position. Figure 10 shows the relative experimental setup.

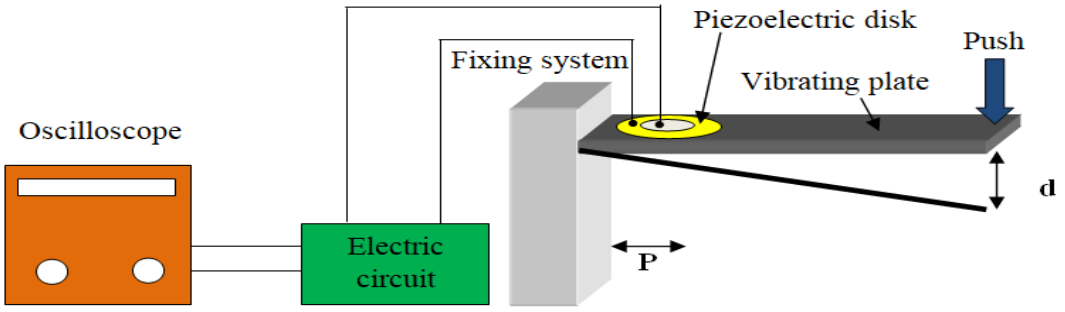

Figure 10. Free excitation experimental setup.

- Forced excitation

The vibrating plate is fixed-free, but a sustained excitation on the fixed end is imposed, in order to initiate forced vibration. The electrical harvested energy is subsequently determined as a function of the frequency. The piezoelectric disk is glued near the plate embedment. Figure 11 shows the relative experimental setup.

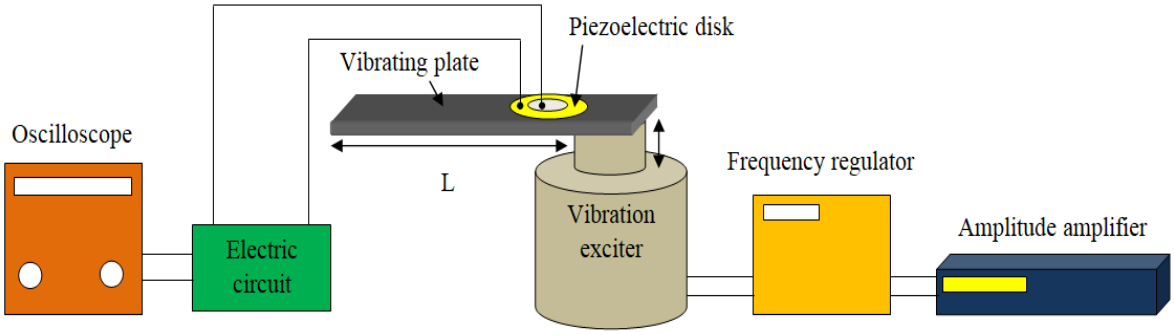

Figure 11. Forced excitation experimental setup.

3. Results and discussion

3.1. Electrical circuit optimization

In this section, we use the configuration presented in Figure 9 (direct excitation experimental setup), and the circuits presented in Figures 6–8 to pinpoint the optimal electric circuit. The experimental results for the different circuits at the different frequencies, 20, 30, 40 and 50 Hz, are

presented in Figure 12 (a–d). The frequency of 10 Hz was excluded due to poor results. The excitation amplitude is fixed at 2 mm. The measured maximum electrical voltage (U), the determined produced electrical energy (W), and the measured capacitor charging time (T) are noted in Table 2.

Table 2. Parameters of the electric circuits at the different excitation frequencies.

	Circuit A			Circuit B			Circuit C		
Frequency (Hz)	U (V)	W (μJ)	T (s)	U (V)	W (μJ)	T (s)	U (V)	W (μJ)	T (s)
20	0.47	0.088	4	0.37	0.068	3	0.227	0.029	4
30	1.8	1.62	4	1.32	0.87	3	0.97	0.52	3
40	3	4.5	4	2.32	2.69	3	1.6	1.420	3
50	5.1	13	4	3.4	5.78	3	2.5	3.46	3

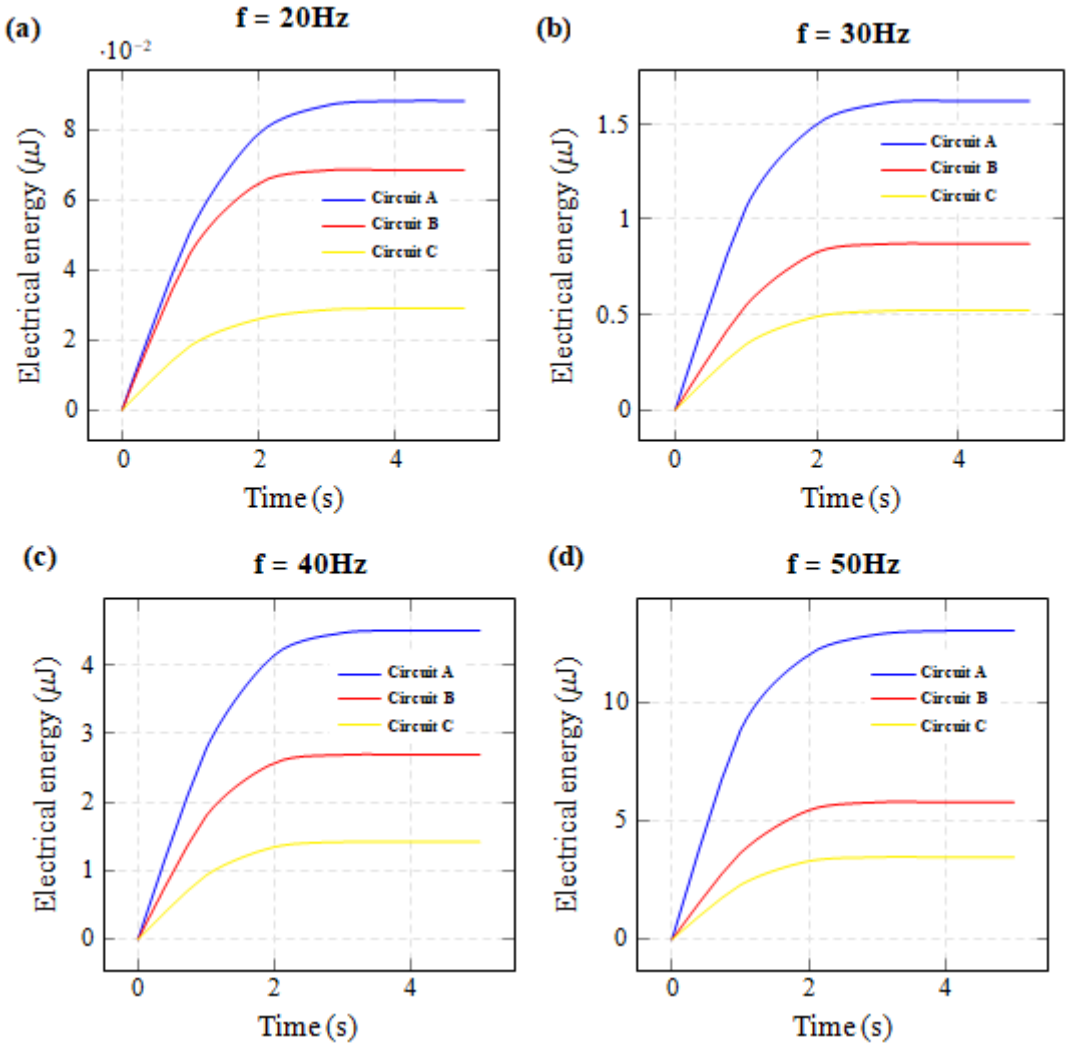

Figure 12. Harvested electrical energy for the different electric circuits at the different excitation frequencies.

In accordance with the obtained results, we note that the recovered electrical energy depends on the configuration of the harvesting electric circuit. Electric circuit (A) presents better produced energy than electric circuit (B), and electric circuit (B) presents better produced energy than electric circuit (C). At the frequency of 20 Hz, electric circuits (A), (B), and (C) deliver very low electrical energy, less than 0.1 μJ. When operated at a frequency of 30 Hz, electric circuits (B) and (C) exhibit low electrical energy output, with values less than 1 μJ, and electric circuit (A) exhibits more than 1.5 μJ. At the frequency of 40 Hz, electric circuit (A) produces 4.5 μJ, electric circuit (B) produces nearly 2.5 μJ, and electric circuit (C) produces nearly 1.5 μJ. With a frequency of 50 Hz, electric circuit (A) harvested 13 μJ, electrical circuit (B) harvested nearly 5 μJ, and electric circuit (C) harvested nearly 3 μJ. Electric circuit (A) is therefore the most interesting, it is retained for the following sections.

3.2. PZT-5H performance

In this section, we use the configuration presented in Figure 9 (direct excitation experimental setup), and circuit (A), to examine the piezoelectric material performance. The experimental results for different excitation amplitudes, 1, 2, 3 and 4 mm, at different excitation frequencies, 10, 20, 30, 40 and 50 Hz, are presented, respectively, in Figure 13 (a–d) and Figure 14. The determined maximal produced electrical energy (Wmax) and the measured capacitor charging time (T) are noted in Table 3.

Table 3. Electrical parameters for the different excitation amplitudes and frequencies.

	Frequency (Hz)									
	10		20		30		40		50	
X (mm)	W (μJ)	T (s)	W (μJ)	T (s)	W (μJ)	T (s)	W (μJ)	T (s)	W (μJ)	T (s)
1	0.00016	2	0.0162	3	0.387	3	1.155	3	4.74	3
2	0.0032	3	0.0882	3	4.74	3	10.125	6	23.12	3
3	0.014	4	0.2312	4	4.74	3	10.125	3	23.12	3
4	0.034	4	0.5	4	8.98	4	21.125	4	36.95	4

Based on the obtained results, the harvested electrical energy strongly depends on the excitation amplitude and the excitation frequency. At the excitation amplitude of 1 mm, the generated electrical energy is around 4.5 μJ at 50 Hz, around 1 μJ at 40 Hz, and less than 1 μJ at 30, 20 and 10 Hz. At the excitation amplitude of 2 mm, the generated electrical energy is around 13 μJ at 50 Hz, around 4 μJ at 40 Hz, around 2 μJ at 30 Hz, and less than 1 μJ at 20 and 10 Hz. At the excitation amplitude of 3 mm, the generated electrical energy is around 23 μJ at 50 Hz, around 10 μJ at 40 Hz, around 4.5 μJ at 30 Hz, and less than 1 μJ at 20 and 10 Hz. At the excitation amplitude of 4 mm, the generated electrical energy is around 37 μJ at 50 Hz, around 21 μJ at 40 Hz, around 9 μJ at 30 Hz, and less than 1 μJ at 20 and 10 Hz. Therefore, increasing the excitation amplitude and frequency gives higher harvested electrical energy.

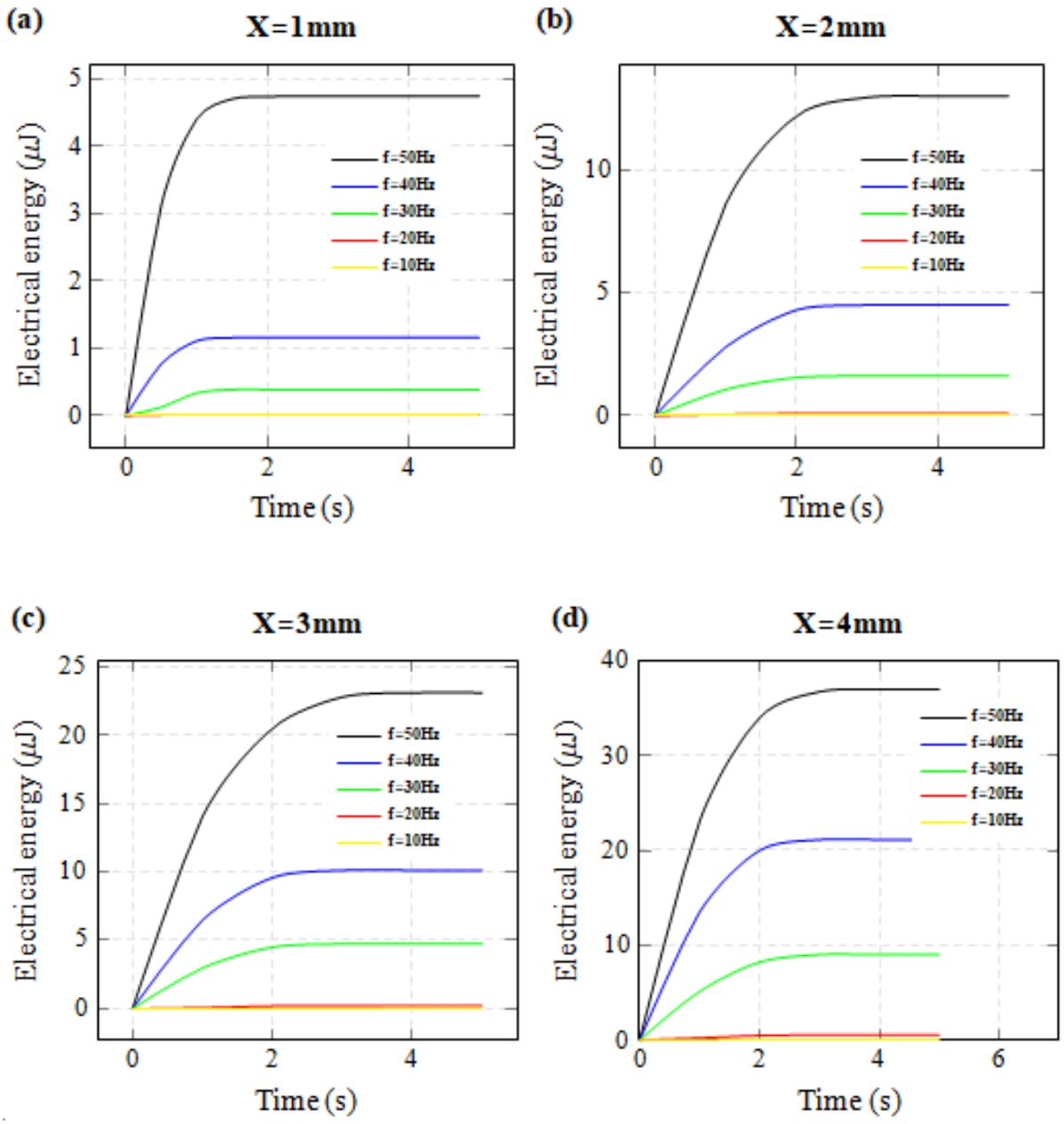

Figure 13. Harvested electrical energy for the different excitation frequencies and amplitudes: (a) X = 1 mm, (b) X = 2 mm, (c) X = 3 mm, (d) X = 4 mm.

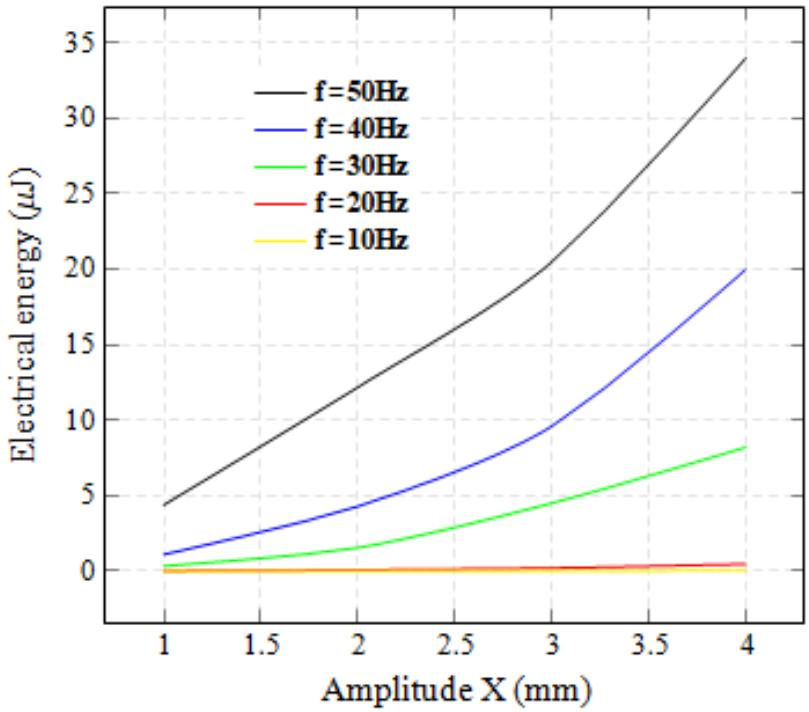

Figure 14. Maximum electrical energy stored in 2s for different amplitudes and excitation frequencies.

3.3. Vibrating plate contribution

During the electric circuit optimization and the piezoelectric disk characterization, the piezoelectric disk is mounted directly on the exciter. To improve the harvested electrical energy, a vibrating plate is introduced. It is fixed-free, and the fixed end is embedded on the exciter. For the free vibration, the vibrating plate is of different materials, and the piezoelectric disk is of different positions, to pinpoint the best plate material and the best disk position. The best excitation displacement is also sought. For the forced vibration, the vibrating plate is of one material and different lengths, and the piezoelectric disk is of one position, to pinpoint the best plate length. The best excitation frequency is also sought.

3.3.1. Free vibration

In this section, we use the configuration presented in Figure 10 (free excitation experimental setup), and circuit (A), to examine the plate material and the disk position effect. The used plates are of ordinary steel, copper, and aluminum. The piezoelectric disk is of different positions on the best plate. The plate dimensions are: length = 150 mm, width = 65 mm, and thickness = 0.5 mm. The experimental results found for the different plate materials, the different piezoelectric disk positions, and the different excitation displacements are illustrated, respectively, in Figures 15–17. The maximum electrical voltage $U(V)$, the maximum electrical energy $W(\mu J)$, and the capacitor charging time (T), are noted, respectively, in Tables 4–6.

Table 4. Electrical parameters for the steel vibrating plate.

Piezoelectric material position P (mm)									
	0 (mm)			104 (mm)			150 (mm)		
d (mm)	U (V)	W (μJ)	T (s)	U (V)	W (μJ)	T (s)	U (V)	W (μJ)	T (s)
5	1.36	0.924	0.186	1.32	0.871	0.23	0.92	0.423	0.2
10	2.64	3.48	0.2	2.38	2.83	0.2	1.54	1.18	0.32
15	3.5	6.12	0.1	2.52	3.17	0.2	2.3	2.64	0.38

Table 5. Electrical parameters for the copper vibrating plate.

Piezoelectric material position P (mm)									
	0 (mm)			104 (mm)			150 (mm)		
d (mm)	U (V)	W (μJ)	T (s)	U (V)	W (μJ)	T (s)	U (V)	W (μJ)	T (s)
5	0.52	0.26	0.2	0.416	0.208	0.1	0.31	0.155	0.3
10	1.06	0.53	0.1	0.98	0.49	0.23	0.88	0.44	0.17
15	1.56	0.78	0.15	1.2	0.6	0.25	1	0.5	0.13

Table 6. Electrical parameters for the aluminum vibrating plate.

Piezoelectric material position P (mm)									
	0 (mm)			104 (mm)			150 (mm)		
d (mm)	U (V)	W (μJ)	T (s)	U (V)	W (μJ)	T (s)	U (V)	W (μJ)	T (s)
5	0.168	0.084	0.2	0.416	0.208	0.1	0.31	0.155	0.3
10	0.616	0.308	0.1	0.98	0.49	0.23	0.88	0.44	0.17
15	1.46	0.73	0.15	1.2	0.6	0.25	1	0.5	0.13

- Material effect

In this study, we investigate the impact of material nature on the recovered electrical energy.

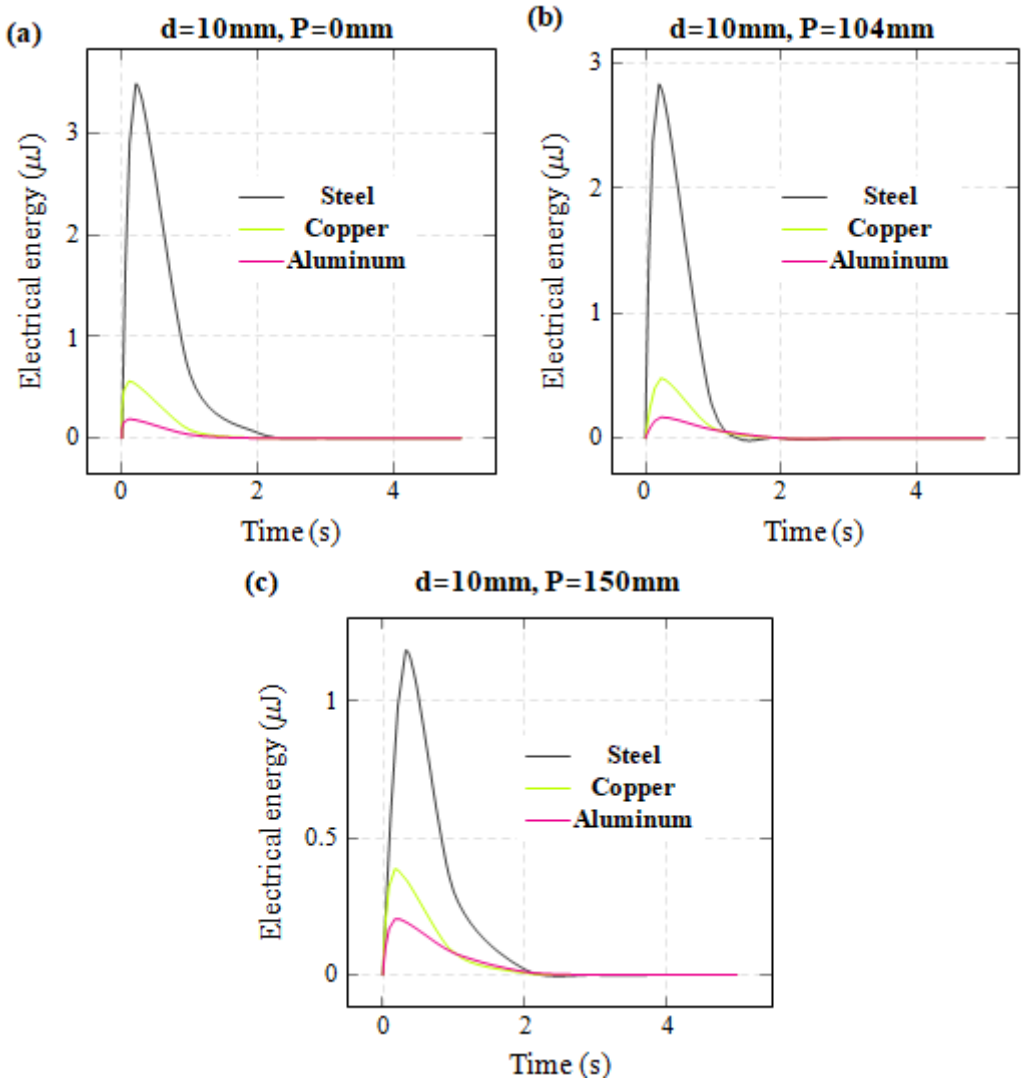

Figure 15. Harvested electrical energy for the different plate materials: (a) P = 0 mm, (b) P = 104 mm, (c) P = 150 mm.

- Position effect

In this study, we examine the impact of the PZT-5H disk position on the recovered electrical energy for each displacement.

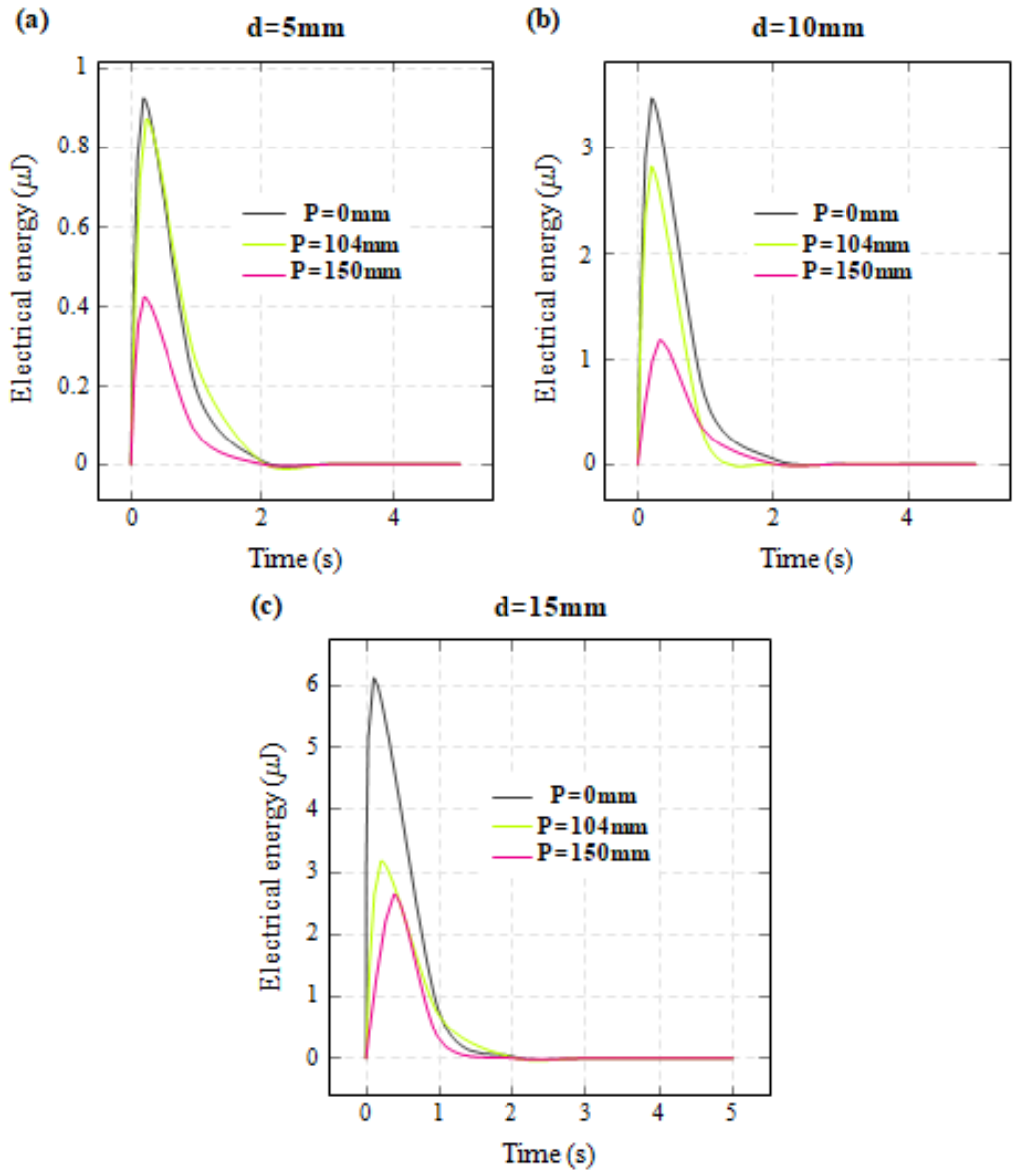

Figure 16. Harvested electrical energy for the different PZT-5H positions: (a) d = 5 mm, (b) d = 10 mm, (c) d = 15 mm.

- Displacement effect

In this study, we examine the impact of displacement on the recovered electrical energy for each position.

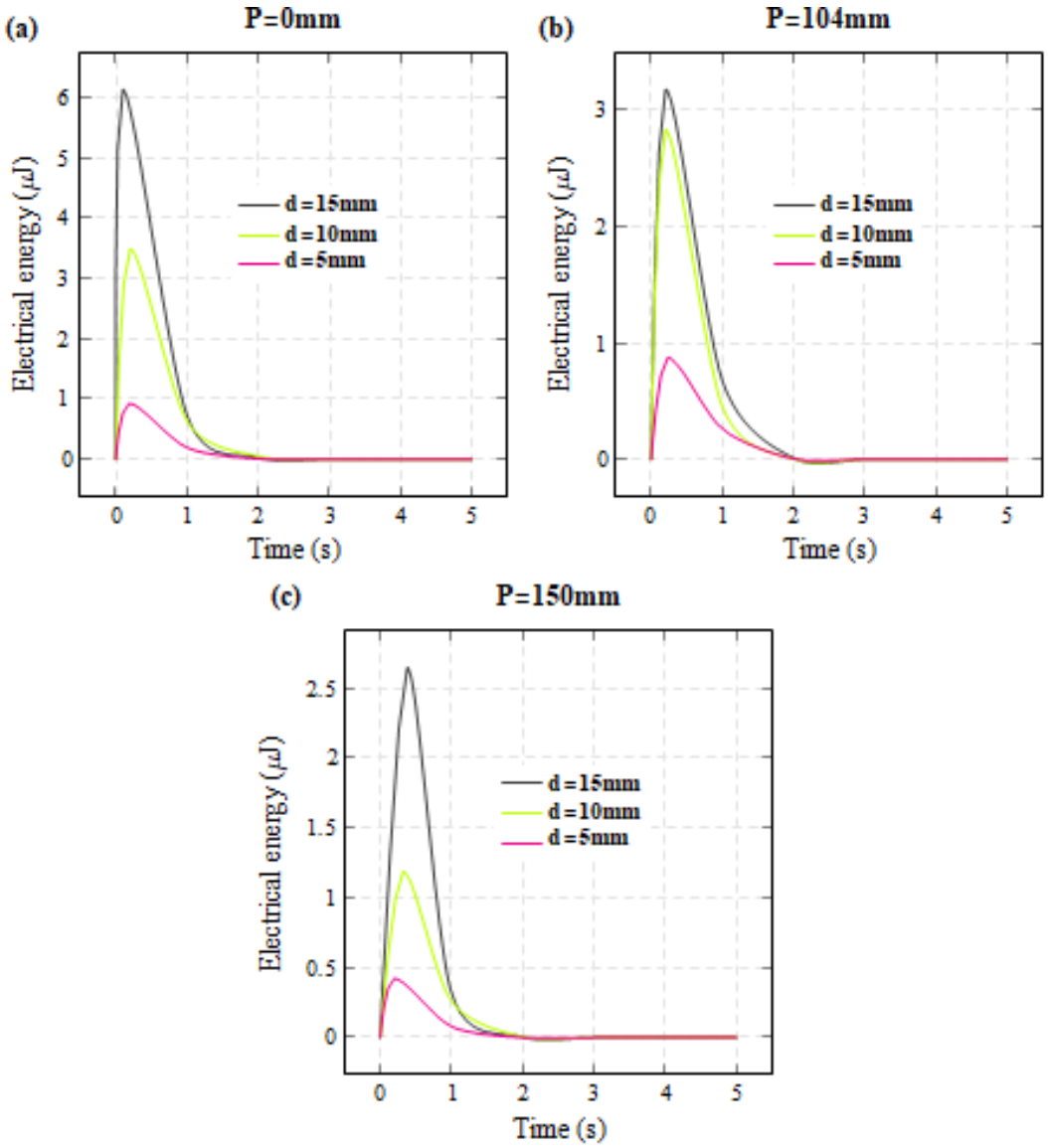

Figure 17. Harvested electrical energy for the different excitation displacements: (a) P = 5 mm, (b) P = 104 mm, (c) P = 150 mm.

In accordance with the obtained results, we note that steel presents better produced electrical energy than copper, and copper presents better produced electrical energy than aluminum. Also, the produced electrical energy depends on the piezoelectric disk position and on the excitation displacement. At the excitation displacement of 10 mm and the piezoelectric disk position of 0 (near the plate embedment), the produced electrical energy using the steel plate is nearly 3.5 μJ, and is under 1 μJ for aluminum and copper plates. At the same excitation displacement and a 104 mm disk position, the produced electrical energy using the steel plate is nearly 2.5 μJ, and is under 1 μJ for aluminum and copper plates. At the same excitation displacement and a 150 mm pizoelectric disk position, the produced electrical energy using the steel plate is nearly 1 μJ, and is under 1 μJ for aluminum and copper plates. The produced electrical energy maximum is around 6 μJ for a steel plate, a piezoelectric disk at the embedment, and a maximal excitation displacement.

3.3.2. Forced vibration

In this section, we use the configuration presented in Figure 11 (forced excitation experimental setup), and circuit (A), to examine the steel plate length effect, with the PZT-5H position at the embedment. The harvested electrical energy and the capacitor charging time are noted in Table 7. Table 8 presents numerical, analytical, and experimental values of the natural frequencies of each plate at the first natural mode. The width and thickness of the steel plates are fixed at 65 and 1.25 mm, respectively. The different lengths are 315, 255, 225 and 170 mm. The excitation amplitude is set at 0.5 mm to avoid excessive stress at the natural frequency. The frequency varies from 10 to 50 Hz. This study seeks higher produced electrical energy.

Table 7. Electrical parameters for the steel vibrating plates.

	L = 315 mm		L = 255 mm		L = 225 mm		L = 170 mm	
Frequency (Hz)	W (μJ)	T (s)	W (μJ)	T (s)	W (μJ)	T (s)	W (μJ)	T (s)
10	3.27	3	1.125	3.5	0.72	2.5	0.0128	2.5
20	0.38	2.5	40.5	3	288	3	2.2	2.5
30	0.722	2.5	18	3	67.28	3	81.92	2.5
40	0.819	2	15.68	2.5	42.32	3	392	2.5
50	1.125	2	32	2	103.68	2	233.28	2.5
Result obtained at resonance	45.31	3	200	3.5	288	3	578	2.5

Table 8. Natural frequencies of the steel vibrating plates.

	L = 315 mm	L = 255 mm	L = 225 mm	L = 170 mm
Experimental f_n (Hz)	10	16	20	36
Analytical f_n (Hz)	10.614	16.197	20.804	36.44
Numerical f_n (Hz)	10.686	16.385	20.5	37.09

- Steel plate with a length of 315 mm

Figure 18(a–c) respectively illustrate the maximum voltage as a function of the excitation frequency, the maximum electrical energy relatively to the excitation frequency, and the electrical energy over time.

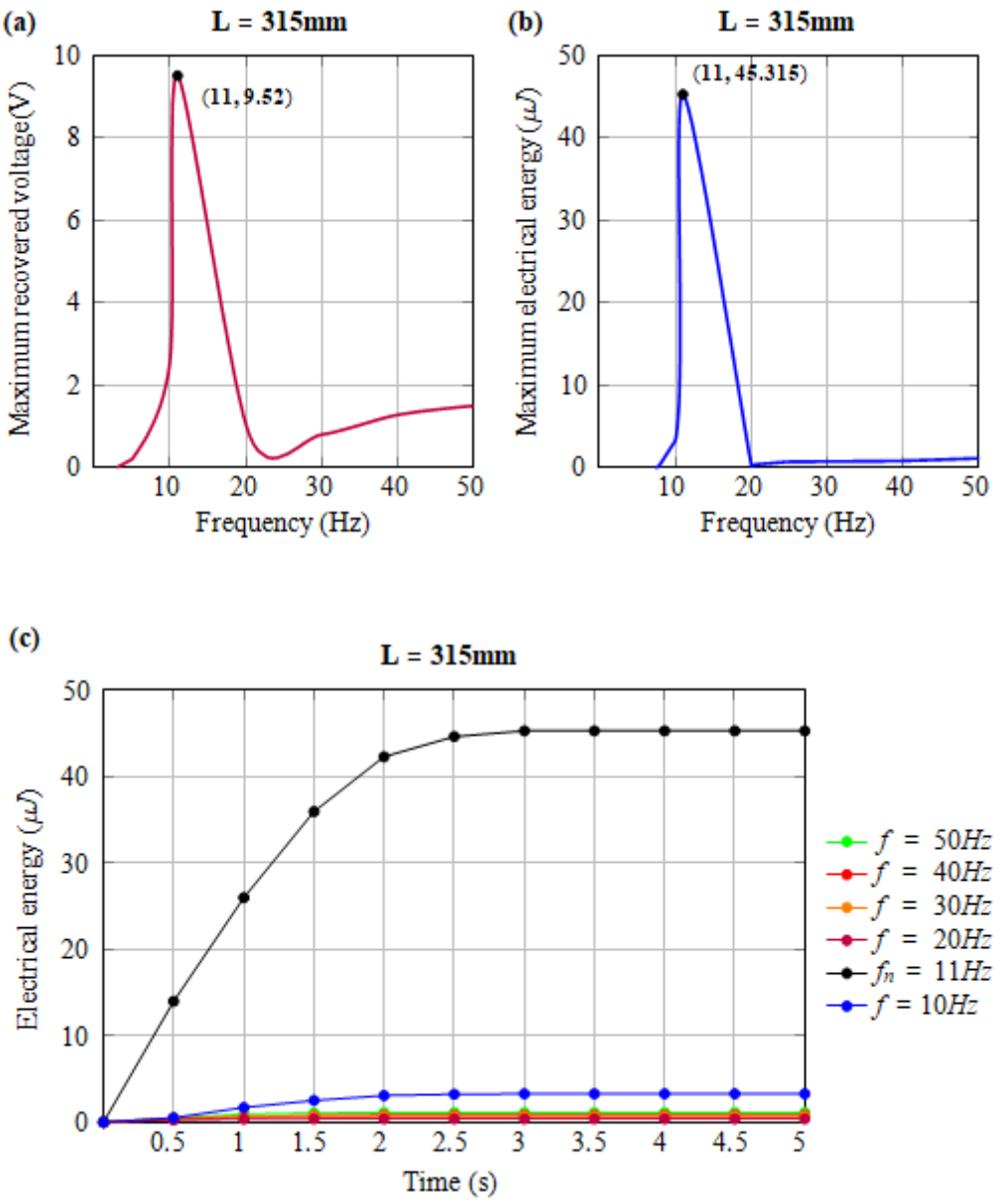

Figure 18. Harvested output at a plate length of 315 mm: (a) maximum voltage as a function of the frequency, (b) maximum electrical energy as a function of the frequency, (c) electrical energy as a function of time.

- Steel plate with a length of 255 mm

Figure 19(a–c) respectively present the maximum voltage as a function of the excitation frequency, the maximum electrical energy relatively to the excitation frequency, and the electrical energy over time.

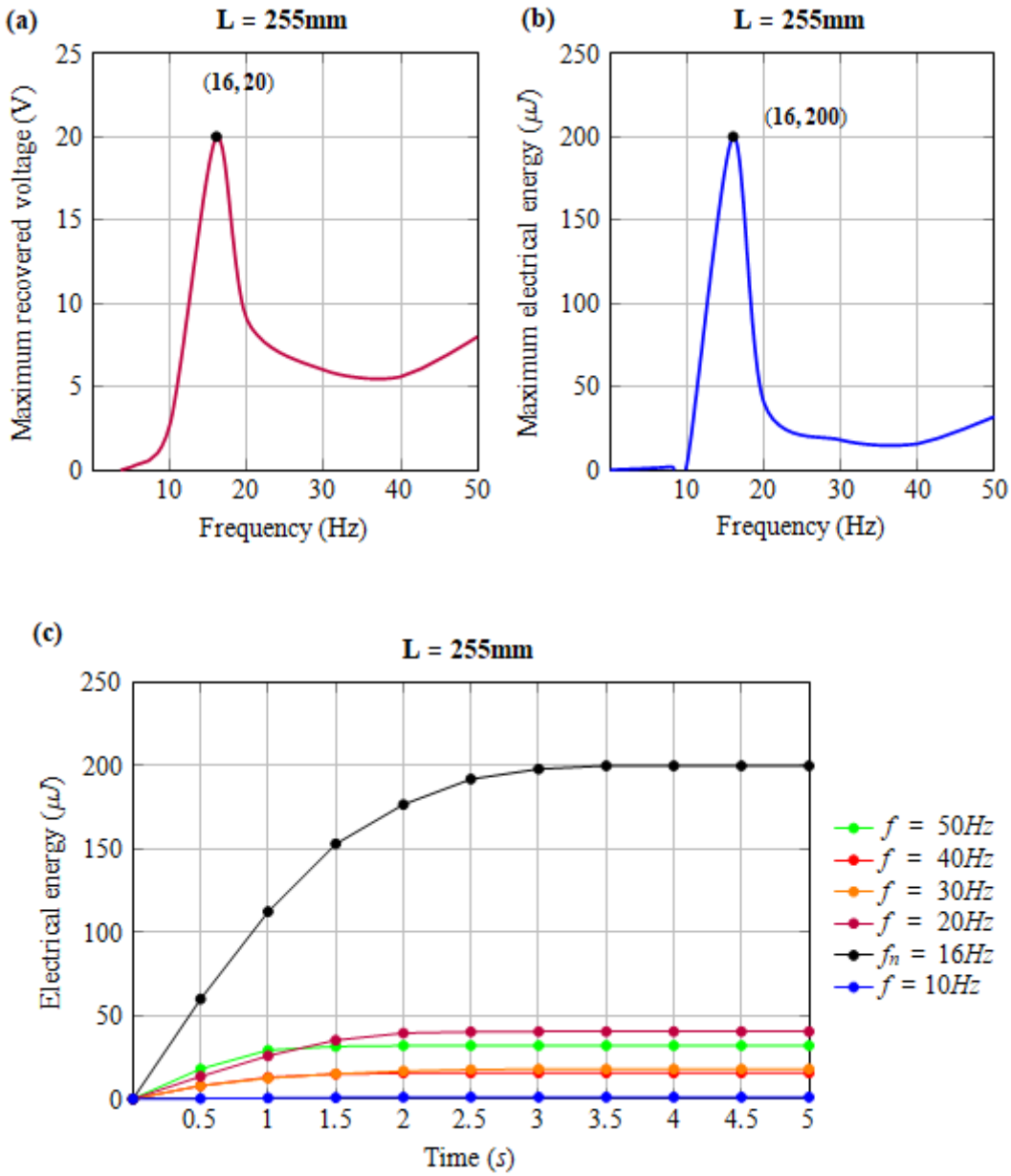

Figure 19. Harvested output at a plate length of 255 mm: (a) maximum voltage as a function of the frequency, (b) maximum electrical energy as a function of the frequency, (c) electrical energy as a function of time.

- Steel plate with a length of 225 mm

Figure 20(a–c) respectively illustrate the maximum voltage as a function of the excitation frequency, the maximum electrical energy relatively to the excitation frequency, and the electrical energy over time.

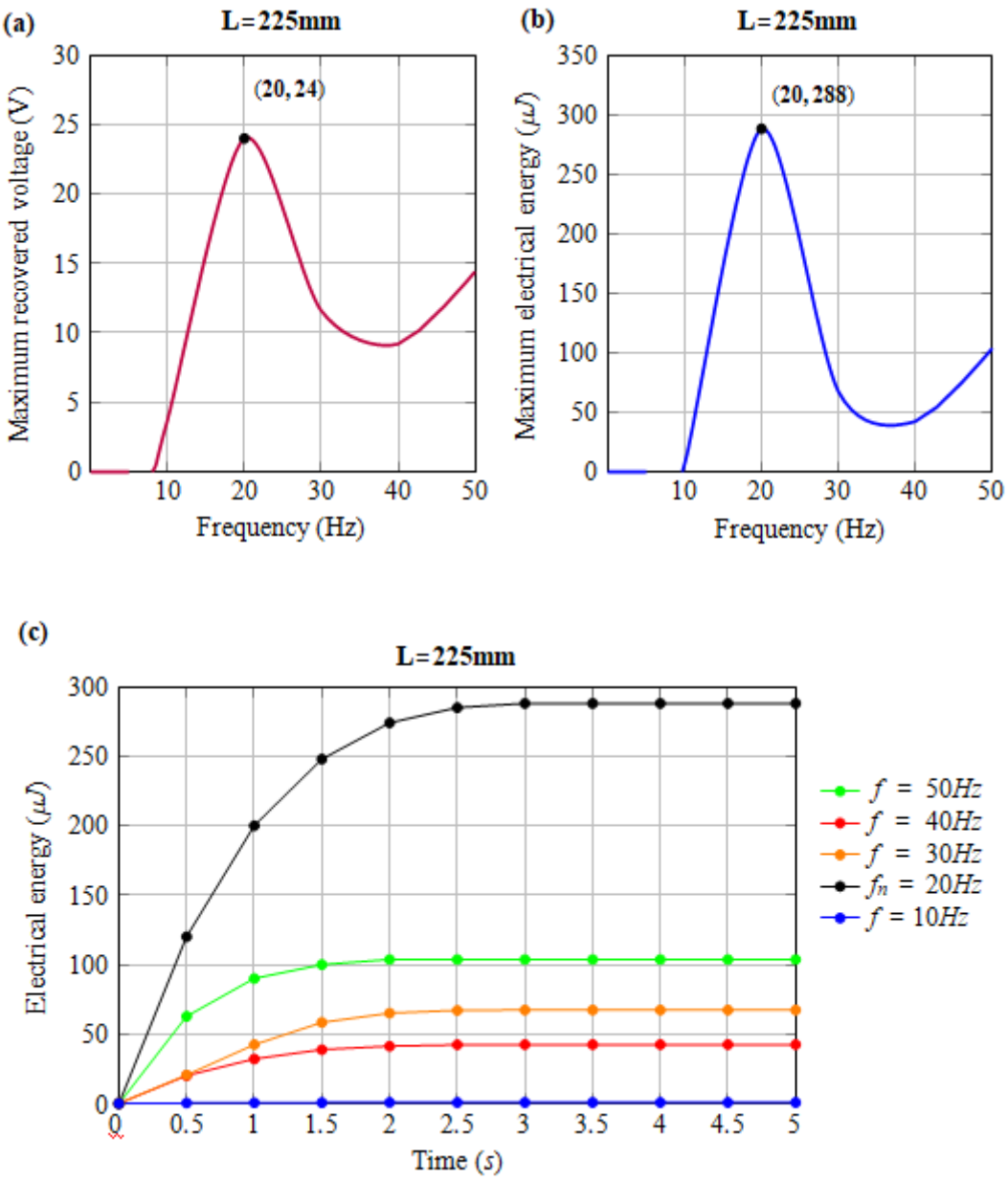

Figure 20. Harvested output at a plate length of 225 mm: (a) maximum voltage as a function of the frequency, (b) maximum electrical energy as a function of the frequency, (c) electrical energy as a function of time.

- Steel plate with a length of 170 mm

Figure 21(a–c) respectively present the maximum voltage as a function of the excitation frequency, the maximum electrical energy relatively to the excitation frequency, and the electrical energy over time.

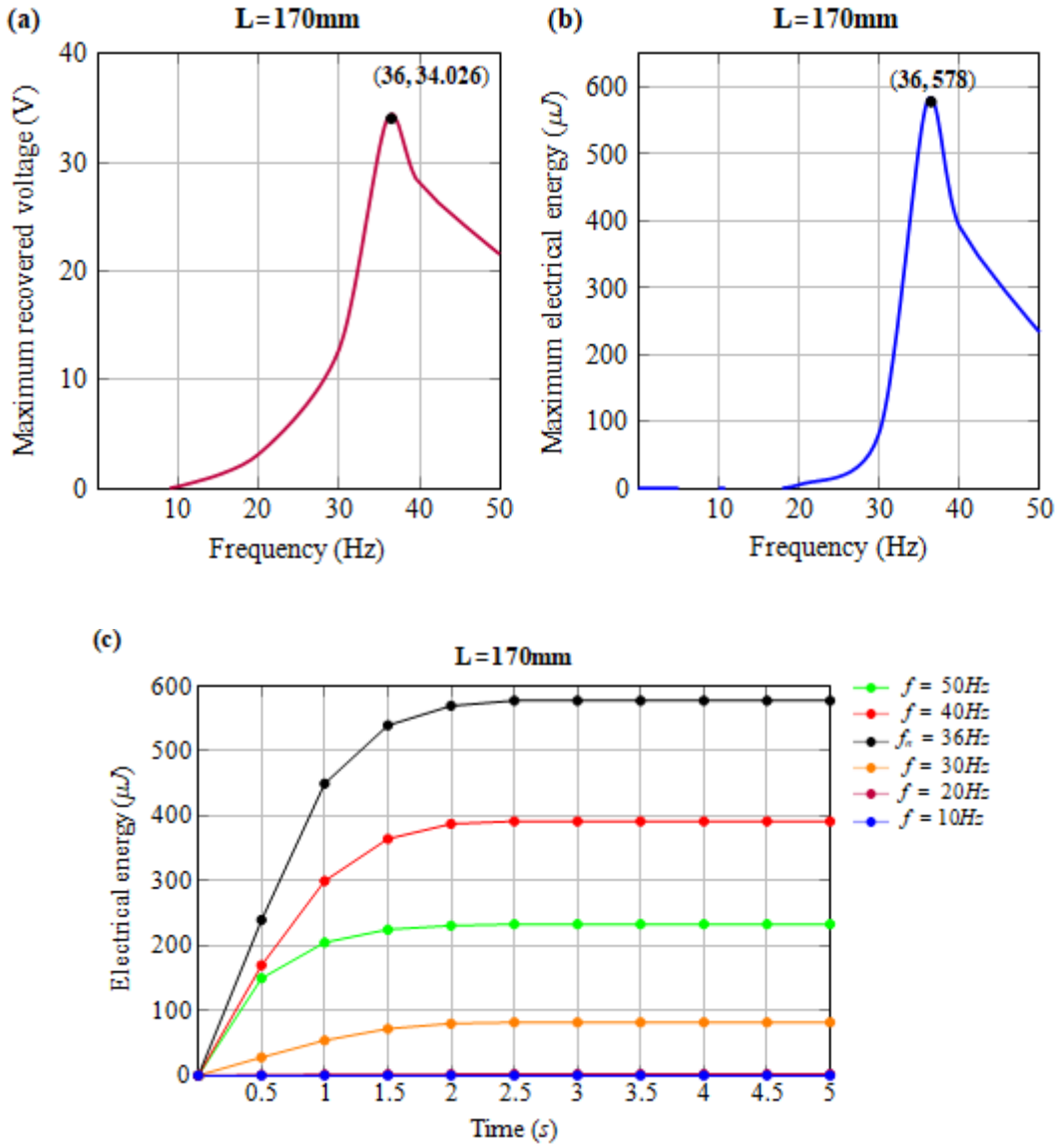

Figure 21. Harvested output at a plate length of 170 mm: (a) maximum voltage as a function of the frequency, (b) maximum electrical energy as a function of the frequency, (c) electrical energy as a function of time.

A substantial enhancement in electrical energy production was seen at the resonance frequency of each plate. The steel plate of length 315 mm produced 45 μJ and 9.5 V at its natural frequency of 10 Hz, and it produced less than 2 μJ and 2 V at all other excitation frequencies. The steel plate with a length of 255 mm generated 200 μJ and 20 V when excited at its natural frequency of 16 Hz, it generated 40.5 μJ and 9 V at the excitation frequency of 20 Hz, 18 μJ and 6 V at the excitation frequency of 30 Hz, 15.7 μJ and 5.6 V at an excitation frequency of 40 Hz, and less than 2 μJ and 2 V at the excitation frequency of 10 Hz. The steel plate of 225 mm in length allowed 288 μJ and 24 V at its natural frequency of 20 Hz, it gave nearly 65 μJ and 11.4 V at the excitation frequency of 30 Hz, nearly 40 μJ and 9 V at the excitation frequency of 40 Hz, nearly 100 μJ and 14.14 V at the excitation frequency of 50 Hz, and less than 4 μJ and 2.8 V at the excitation frequency of 10 Hz. The plate of 170 mm in length gave 578 μJ and 34 V when driven at its natural frequency of 36 Hz, it allowed 2.2 μJ

and 2.09 V at the excitation frequency of 20 Hz, nearly 81 μJ and 13 V at an excitation frequency of 30 Hz, about 392 μJ and 28 V at 40 Hz, nearly 233 μJ and 21.5 V at 50 Hz, and less than 1 μJ and 2 V at the excitation frequency of 10 Hz. The maximum electrical energy produced is around 578 μJ and the maximum recovered voltage is about 34 V for the shortest steel plate at its natural frequency. Therefore, a shorter steel plate with a natural frequency around 50 Hz would be interesting.

- Resonance tuning effect

This section looks into a steel vibrating plate that significantly boosts harvested electrical energy using piezoelectric effect within the frequency range of 0 to 50 Hz. Building on previous results, the harvested electrical energy increases greatly at the plate natural frequency which should be the highest possible. To identify the optimal dimensions of the steel plate that generates maximum electrical energy within the frequency range of 0 to 50 Hz, we set the thickness to 1.25 mm and the width to 65 mm. We then determined the length at which the natural frequency of the plate coincides with 50 Hz. Through analytical and numerical calculations, the optimal length for the steel plate was found around 145 mm. Figure 22 describes the ideal steel plate. Figure 23(a–c) highlights the maximum voltage as a function of the excitation frequency, the maximum energy relatively to the excitation frequency, and the electrical energy over time, respectively, for a steel plate with a length of 145 mm.

Figure 22. Ideal steel plate: length = 145 mm, width = 65 mm, thickness = 1.25 mm.

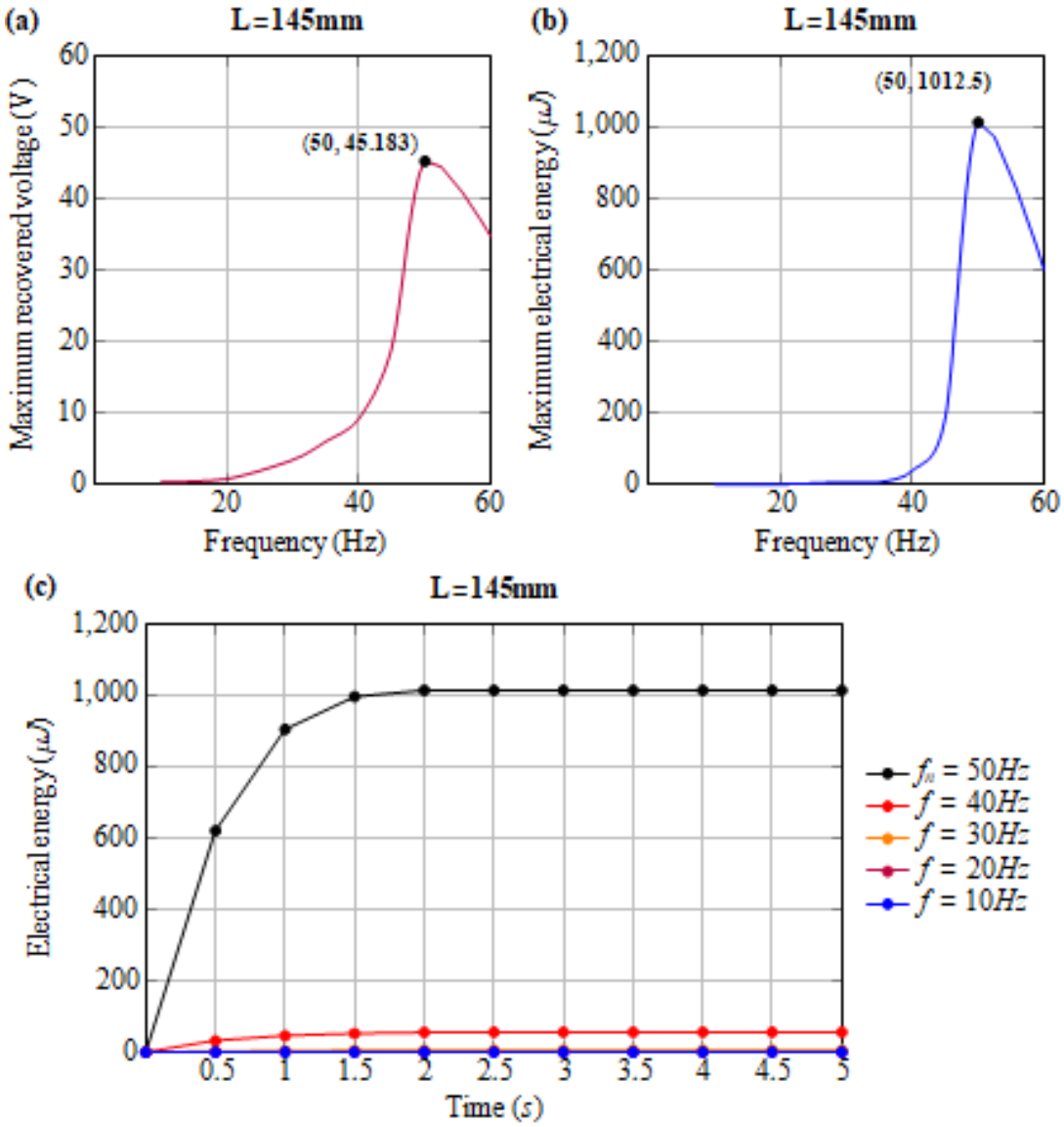

Figure 23. Harvested electrical energy for the ideal steel plate: (a) maximum voltage as a function of the frequency, (b) maximum electrical energy as a function of the frequency, (c) electrical energy as a function of time.

Based on the findings, the ideal steel plate achieved a maximum harvested electrical energy of 1012.5 μJ and a peak voltage of 45 V at its natural frequency of 50 Hz. It is huge and capable of powering several electronic devices. The harvested electrical energy at the excitation frequency of 40 Hz is 56 μJ, which is about 18 times less, but it is still enough strong. At the excitation frequency of 30 Hz, the obtained electrical energy is about 5 μJ, which is still interesting. The harvested electrical energies and the recovered voltages are, respectively, less than 1 μJ and 1.5 V at the excitation frequencies of 20 and 10 Hz, which are too low to be considered.

4. Conclusions

The field of energy harvesting has grown rapidly with the huge development of low-power devices and the Internet of Things (IoT). With the intent of harvesting electrical energy for self-powered devices, piezoelectric micro-generator technology is considered.

In this study, we proposed several electrical and mechanical improvements to enhance the electrical energy produced through piezoelectricity. To determine the best electrical configuration to harvest piezoelectric energy, three harvesting electric circuits were proposed and tested using a piezoelectric disk mounted directly on a vibration exciter, using an epoxy adhesive. The harvested electrical energy by each circuit was determined at different excitation frequencies, from 20 to 50 Hz, with an excitation amplitude of 2 mm. The favorable electric circuit consisting of two Schottky diodes and a capacitor allowed a harvested electrical energy around 35 μJ at an excitation frequency of 50 Hz, and it was retained for the whole study. The best circuit was then used to characterize the piezoelectric material. Increasing the excitation amplitude and frequency was found to give higher harvested electrical energy. To enhance the obtained electrical energy, a fixed-free metallic plate was used. First, free vibration was tried, imposing an excitation displacement of different values to the free end of the plate. The plate was made of different materials: Copper, aluminum, and steel. The piezoelectric material was mounted on different positions on the plate, using an epoxy adhesive. The harvested electrical energy was determined for each plate material, each piezoelectric material position, and each excitation displacement. The highest harvested energy was around 6 μJ for a steel plate, a PZT-5H disk position at the embedment, and a maximal excitation displacement. Second, forced vibration was tried, imposing an excitation amplitude of 0.5 mm at different excitation frequencies, from 10 to 50 Hz, to the fixed end of the plate. The plate was of different lengths. The highest harvested energy was around 540 μJ and the highest peak voltage was about 33 V. Third, we showed that it is possible to further increase the harvested electrical energy by tuning the plate resonance to 50 Hz. The harvested energy is then around 1010 μJ and the recovered voltage is about 45 V, which is capable of powering several electronic devices at once.

The obtained results allow optimizing piezoelectric energy harvesting, regarding vibrational excitation, the mechanical system, the piezoelectric transducer, and the electric circuit, toward supplying low-power devices for different applications. Table 9 presents a comparison between the related studies on piezoelectric energy harvesting and the research work discussed in this paper.

Table 9. Summary of related works based on piezoelectric energy harvesting.

References	Materials	Dimensions	Mechanical input	Electrical output
[53]	PZT-5A	(33.5 × 2 × 0.25) mm	12 Hz	65 μW
[54]	PZT-5A	(60 × 84 × 2.5) mm	262–263 Hz	4811.8 μW
[55]	PVDF	(25 × 16 × 0.2) mm	14 Hz	16 μW
[56]	PZT-Silver-Copper	(80 × 33 × 0.2) mm	23.29 Hz	7290 μW/cm^3
[57]	PZT-5A	(100 × 60 × 30) mm	4 m/s	4000 μW
[58]	PVDF	(30 × 16 × 0.1) mm	8.83 Hz	73 μW
[59]	PVDF	(20 × 10 × 0.3) mm	8.2 Hz	12.2 μW
This study	PZT-5H	(145 × 65 × 1.25) mm	50 Hz	1012.5 μJ

Use of AI tools declaration

The authors declare they have not used Artificial Intelligence (AI) tools in the creation of this article.

Acknowledgments

This work is partially supported by the Tunisian-Moroccan mixed technical committee for cooperation in research and innovation, within the project: Multi-functional nanomaterials for energy and environment (NanoFor2E).

Conflict of interest

The authors declare no conflict of interest.

Author contributions

The contributions of the authors to this work are as follows: Amine BEN ALAYA—methodology, analysis, experimental evaluations; Charfeddine MRAD—methodology, supervision, validation; Férid KOURDA—conceptualization, investigation.

References

1. Rejeb A, Rejeb K, Treiblmaier H, et al. (2023) The Internet of Things (IoT) in healthcare: Taking stock and moving forward. *Int Things* 22: 100721. https://doi.org/10.1016/j.iot.2023.100721
2. Sarker IH, Khan AI, Abushark YB, et al. (2023) Internet of things (IoT) security intelligence: A comprehensive overview, machine learning solutions and research directions. *Mobile Netw Appl* 28: 296–312. https://doi.org/10.1007/s11036-022-01937-3
3. Davis D, Birnbaum L, Ben-Ishai P, et al. (2023) Wireless technologies, non-ionizing electromagnetic fields and children: Identifying and reducing health risks. *Curr Probl Pediatr Adolesc Health Care* 53: 101374. https://doi.org/10.1016/j.cppeds.2023.101374
4. Butt FA, Chattha JN, Ahmad J, et al. (2022) On the integration of enabling wireless technologies and sensor fusion for next-generation connected and autonomous vehicles. *IEEE Access* 10: 14643–14668. https://doi.org/10.1109/ACCESS.2022.3145972
5. Azarpour A, Mohammadzadeh O, Rezaei N, et al. (2022) Current status and future prospects of renewable and sustainable energy in North America: Progress and challenges. *Energy Convers Manage* 269: 115945. https://doi.org/10.1016/j.enconman.2022.115945
6. Hosseini SE (2020) An outlook on the global development of renewable and sustainable energy at the time of COVID-19. *Energy Res Soc Sci* 68: 101633. https://doi.org/10.1016/j.erss.2020.101633
7. Jaiswal KK, Chowdhury CR, Yadav D, et al. (2022) Renewable and sustainable clean energy development and impact on social, economic, and environmental health. *Energy Nexus* 7: 100118. https://doi.org/10.1016/j.nexus.2022.100118

8. Ngoc DD, Trung KD, Minh PV, et al. (2024) Assessing factors influencing green hydrogen conversion at Vietnam's gas turbine power plants using combined SWOT-AHP analysis method. *AIMS Energy* 12: 1054–1074. https://doi.org/10.3934/energy.2024050
9. Toka KA, Nougbléga Y, Amou KA (2024) Optimization of hybrid photovoltaic-thermal systems integrated into buildings: Impact of bi-fluid exchangers and filling gases on the thermal and electrical performances of solar cells. *AIMS Energy* 12: 1075–1095. https://doi.org/10.3934/energy.2024051
10. Larranaga A, Valor C (2022) Consumers' categorization of eco-friendly consumer goods: An integrative review and research agenda. *Sustainable Prod Consum* 34: 518–527. https://doi.org/10.1016/j.spc.2022.10.005
11. Hossein M, Asha R, Bakari R, et al. (2023) Exploring eco-friendly approaches for mitigating pharmaceutical and personal care products in aquatic ecosystems: A sustainability assessment. *Chemosphere* 316: 137715. https://doi.org/10.1016/j.chemosphere.2022.137715
12. Bilgen SELÇ UK (2014) Structure and environmental impact of global energy consumption. *Renewable Sustainable Energy Rev* 38: 890–902. https://doi.org/10.1016/j.rser.2014.07.004
13. Osman AI, Chen L, Yang M, et al. (2023) Cost, environmental impact, and resilience of renewable energy under a changing climate: A review. *Environ Chem Lett* 21: 741–764. https://doi.org/10.1007/s10311-022-01532-8
14. Wang Y, Guo T, Tian Z, et al. (2022) MXenes for energy harvesting. *Adv Mater* 34: 2108560. https://doi.org/10.1002/adma.202108560
15. Panda S, Hajra S, Mistewicz K, et al. (2022) Piezoelectric energy harvesting systems for biomedical applications. *Nano Energy* 100: 107514. https://doi.org/10.1016/j.nanoen.2022.107514
16. Sezer N, Koç M (2021) A comprehensive review on the state-of-the-art of piezoelectric energy harvesting. *Nano Energy* 80: 105567. https://doi.org/10.1016/j.nanoen.2020.105567
17. Dai B, Guo J, Gao C, et al. (2023) Recent advances in efficient photocatalysis via modulation of electric and magnetic fields and reactive phase control. *Adv Mater* 35: 2210914. https://doi.org/10.1002/adma.202210914
18. Kamel NA (2022) Bio-piezoelectricity: fundamentals and applications in tissue engineering and regenerative medicine. *Biophys Rev* 14: 717–733. https://doi.org/10.1007/s12551-022- 00969-z
19. Ghasemian MB, Daeneke T, Shahrbabaki Z, et al. (2020) Peculiar piezoelectricity of atomically thin planar structures. *Nanoscale* 12: 2875–2901. https://doi.org/10.1039/C9NR08063E
20. Gao A, Remsing RC (2022) Self-consistent determination of long-range electrostatics in neural network potentials. *Nat Commun* 13: 1572. https://doi.org/10.1038/s41467-022-29243-2
21. Alabugin IV, Kuhn L, Krivoshchapov NV, et al. (2021) Anomeric effect, hyperconjugation and electrostatics: Lessons from complexity in a classic stereoelectronic phenomenon. *Chem Soc Rev* 50: 10212–10252. https://doi.org/10.1039/D1CS00564B
22. Moya SM, Botella NB (2021) Review of techniques to reduce and prevent carbonate scale. Prospecting in water treatment by magnetism and electromagnetism. *Water* 13: 2365. https://doi.org/10.3390/w13172365
23. Córdova C, Ohmori K (2024) Quantum duality in electromagnetism and the fine structure constant. *Phys Rev D* 109: 105019. https://doi.org/10.1103/PhysRevD.109.105019

24. Joo H, Lee KY, Lee JH (2022) Piezo/triboelectric effect driven self-powered gas sensor for environmental sensor networks. *Energy Technol* 10: 2200113. https://doi.org/10.1002/ente.202200113
25. Pan S, Zhang Z (2019) Fundamental theories and basic principles of triboelectric effect: A review. *Friction* 7: 2–17. https://doi.org/10.1007/s40544-018-0217-7
26. Dai B, Gao C, Guo J, et al. (2024) A robust pyro-phototronic route to markedly enhanced photocatalytic disinfection. *Nano Lett* 24: 4816–4825. https://doi.org/10.1021/acs.nanolett.3c05098
27. Săvescu C, Comeagă D, Morega AM, et al. (2022) Experimental tests with piezoelectric harvester for tuning resonant frequency to vibrating source. *Rev Roum Sci Techn—Sér Electrotech Energ* 67: 457–460. https://orcid.org/0000-0001-9578-1222
28. Zou Y, Gai Y, Tan P, et al. (2022) Stretchable graded multichannel self-powered respiratory sensor inspired by shark gill. *Fundam Res* 2: 619–628. https://doi.org/10.1016/j.fmre.2022.01.003
29. Shaukat H, Ali A, Bibi S, et al. (2023) A Review of the recent advances in piezoelectric materials, energy harvester structures, and their applications in analytical chemistry. *Appl Sci* 13: 1300. https://doi.org/10.3390/app13031300
30. Goldsmid HJ (2018) Conversion efficiency and figure-of-merit. In: *CRC Handbook of Thermoelectrics*, CRC Press, 19–26. https://doi.org/10.1201/9781420049718
31. Li C, Jiang G, Yu J, et al. (2023) Fluorination enhances NIR-II emission and photothermal conversion efficiency of phototheranostic agents for imaging-guided cancer therapy. *Adv Mater* 35: 2208229. https://doi.org/10.1002/adma.202208229
32. Peng Y, Zhang L, Li Z, et al. (2023) Influences of wire diameters on output power in electromagnetic energy harvester. *Int J Precis Eng Manuf Green Tech* 10: 205–216. https://doi.org/10.1007/s40684-022-00446-8
33. Cai C, Saeedifard M, Wang J, et al. (2022) A cost-effective segmented dynamic wireless charging system with stable efficiency and output power. *IEEE Trans Power Electron* 37: 8682–8700. https://doi.org/10.1109/TPEL.2022.3143128
34. Logeshwaran J, Ramkumar M, Kiruthiga T, et al. (2022) The role of integrated structured cabling system (ISCS) for reliable bandwidth optimization in high-speed communication network. *ICTACT J Commun Technol* 13: 2635–2639. https://doi.org/10.21917/ijct.2022.0389
35. Ansari S, Zhang J, Singh RE, et al. (2022) A review of stabilization methods for DCMG with CPL, the role of bandwidth limits and droop control. *Protect Control Mod Power Syst* 7: 1–12. https://doi.org/10.1186/s41601-021-00222-x
36. Li H, Tian C, Deng ZD (2014) Energy harvesting from low frequency applications using piezoelectric materials. *Appl Phys Rev* 1:041301. https://doi.org/10.1063/1.4900845
37. Han HS, Duong TA, Ahn CW, et al. (2023) A brief review on piezoelectrics-based paint sensors. *J Korean Inst Electr Electron Mater Eng* 36: 433–441. https://doi.org/10.4313/JKEM.2023.36.5.2
38. Maurya D, Kumar P, Khaleghian S, et al. (2018) Energy harvesting and strain sensing in smart tire for next generation autonomous vehicles. *Appl Energy* 232: 312–322. https://doi.org/10.1016/j.apenergy.2018.09.183

39. Rupp CJ, Evgrafov A, Maute K, et al. (2009) Design of piezoelectric energy harvesting systems: A topology optimization approach based on multilayer plates and shells. *J Intell Mater Syst Struct* 20: 1923–1939. https://doi.org/10.1177/1045389X09341200
40. Lefeuvre E, Badel A, Richard C, et al. (2006) A comparison between several vibration-powered piezoelectric generators for standalone systems. *Sens Actuators A Phys* 126: 405–416. https://doi.org/10.1016/j.sna.2005.10.043
41. Song J, Sun G, Zeng X, et al. (2022) Piezoelectric energy harvester with double cantilever beam undergoing coupled bending-torsion vibrations by width-splitting method. *Sci Rep* 12: 583. https://doi.org/10.1038/s41598-021-04476-1
42. Baek C, Wang JE, Ryu S, et al. (2017) Facile hydrothermal synthesis of $BaZr_xTi_{1-x}O_3$ nanoparticles and their application to a lead-free nanocomposite generator. *RSC Adv* 7: 2851–2856. https://doi.org/10.1039/C6RA26285F
43. Han JH, Park KI, Jeong CK (2019) Dual-structured flexible piezoelectric film energy harvesters for effectively integrated performance. *Sensors* 19: 1444. https://doi.org/10.3390/s19061444
44. Lee J, Kim S, Oh J, et al. (2012) A self-powering system based on tire deformation during driving. *Int J Automot Technol* 13: 963–969. https://doi.org/10.1007/s1223901200980
45. Baker J, Roundy S, Wright P (2005) Alternative geometries for increasing power density in vibration energy scavenging for wireless sensor networks. In: *3rd International Energy Conversion Engineering Conference*, 5617. https://doi.org/10.2514/6.2005-5617
46. Sterken T, Baert K, Van Hoof C, et al. (2004) Comparative modelling for vibration scavengers [MEMS energy scavengers]. *Sensors 2004 IEEE*, Vienna, Austria, 1249–1252. https://doi.org/10.1109/ICSENS.2004.1426407
47. Wang R, Tang E, Yang G, et al. (2020) Experimental research on dynamic response of PZT-5H under impact load. *Ceram Int* 46: 2868–2876. https://doi.org/10.1016/j.ceramint.2019.09.280
48. Beeby SP, Tudor MJ, White NM (2006) Energy harvesting vibration sources for microsystems applications. *Meas Sci Technol* 17: R175. https://doi.org/10.1088/0957-0233/17/12/R01
49. Li P, Wen Y, Liu P, et al. (2010) A magnetoelectric energy harvester and management circuit for wireless sensor network. *Sens Actuators A Phys* 157: 100–106. https://doi.org/10.1016/j.sna.2009.11.007
50. Sriphan S, Vittayakorn N (2022) Hybrid piezoelectric-triboelectric nanogenerators for flexible electronics: Recent advances and perspectives. *J Sci Adv Mater Devices* 7: 100461. https://doi.org/10.1016/j.jsamd.2022.100461
51. Liu Y, Tian G, Wang Y, et al. (2009) Active piezoelectric energy harvesting: General principle and experimental demonstration. *J Intell Mater Syst Struct* 20: 575–585. https://doi.org/10.1177/1045389X08098195
52. Allamraju KV, Srikanth K (2016) Design and experimental study of novel piezoelectric vibration energy impact mass harvester. *Proc Eng* 144: 560–567. https://doi.org/10.1016/j.proeng.2016.05.042
53. Fu H, Yeatman EM (2017) Broadband rotational energy harvesting using bistable mechanism and frequency up-conversion. In: *2017 IEEE 30th International Conference on Micro Electro Mechanical Systems (MEMS)*, Las Vegas, NV, USA, 853–856. https://doi.org/10.1109/MEMSYS.2017.7863542

54. Fairuz WNM, Nawi IM, Ahmad MR, et al. (2024) Design analysis and simulation of serpentine-shaped piezoelectric cantilever beam for pipeline vibration-based energy harvester. *AIMS Energy* 12: 561–599. https://doi.org/10.3934/energy.2024027
55. Jiang Y, Shiono S, Hamada H, et al. (2010) Low-frequency energy harvesting using a laminated PVDF cantilever with a magnetic mass. *Power MEMS* 30: 375–378.
56. Xu Q, Gao A, Li Y, et al. (2022) Design and optimization of piezoelectric cantilever beam vibration energy harvester. *Micromachines* 13: 675. https://doi.org/10.3390/mi13050675
57. Kwon SD (2010) A T-shaped piezoelectric cantilever for fluid energy harvesting. *Appl Phys Lett,* 97. https://doi.org/10.1063/1.3503609
58. Xiong C, Wu N, He Y, et al. (2023) Nonlinear energy harvesting by piezoelectric bionic 'M' shape generating beam featured in reducing stress concentration. *Micromachines* 14: 1007. https://doi.org/10.3390/mi14051007
59. Derakhshani M, Momenzadeh N, Berfield TA (2021) Analytical and experimental study of a clamped-clamped, bistable buckled beam low-frequency PVDF vibration energy harvester. *J Sound Vib* 497: 115937. https://doi.org/10.1016/j.jsv.2021.115937

AIMS Press